JACS Au
AN OPEN ACCESS JOURNAL OF THE AMERICAN CHEMICAL SOCIETY

pubs.acs.org/jacsau

Article

Antitumor Effects of a Distinct Sonodynamic Nanosystem through Enhanced Induction of Immunogenic Cell Death and Ferroptosis with Modulation of Tumor Microenvironment

Haitao Yuan, Jingbo Ma, Wei Huang, Ping Gong, Fei Shi, Xiaolong Xu, Chunjin Fu, Xiaoxian Wang, Yin Kwan Wong, Ying Long, Xin Sun,* Weihua Li,* Zhijie Li,* and Jigang Wang*

Cite This: *JACS Au* 2023, 3, 1507−1520

Read Online

ACCESS | Metrics & More | Article Recommendations | Supporting Information

ABSTRACT: Sonodynamic therapy (SDT) holds great promise to be applied for cancer therapy in clinical settings. However, its poor therapeutic efficacy has limited its applications owing to the apoptosis-resistant mechanism of cancer cells. Moreover, the hypoxic and immunosuppressive tumor microenvironment (TME) also weakens the efficacy of immunotherapy in solid tumors. Therefore, reversing TME remains a formidable challenge. To circumvent these critical issues, we developed an ultrasound-augmented strategy to regulate the TME by utilizing an HMME-based liposomal nanosystem (HB liposomes), which can synergistically promote the induction of ferroptosis/apoptosis/immunogenic cell death (ICD) and initiate the reprograming of TME. The RNA sequencing analysis demonstrated that apoptosis, hypoxia factors, and redox-related pathways were modulated during the treatment with HB liposomes under ultrasound irradiation. The in vivo photoacoustic imaging experiment showed that HB liposomes enhanced oxygen production in the TME, alleviated TME hypoxia, and helped to overcome the hypoxia of the solid tumors, consequently improving the SDT efficiency. More importantly, HB liposomes extensively induced ICD, resulting in enhanced T-cell recruitment and infiltration, which normalizes the immunosuppressive TME and facilitates antitumor immune responses. Meanwhile, the HB liposomal SDT system combined with PD1 immune checkpoint inhibitor achieves superior synergistic cancer inhibition. Both in vitro and in vivo results indicate that the HB liposomes act as a sonodynamic immune adjuvant that is able to induce ferroptosis/apoptosis/ICD via generated lipid-reactive oxide species during the SDT and reprogram TME due to ICD induction. This sonodynamic nanosystem integrating oxygen supply, reactive oxygen species generation, and induction of ferroptosis/apoptosis/ICD is an excellent strategy for effective TME modulation and efficient tumor therapy.

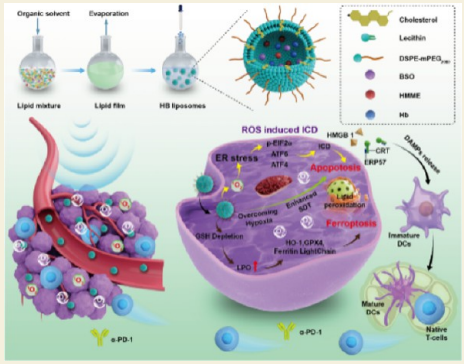

KEYWORDS: *sonodynamic therapy, immunogenic cell death, ferroptosis, cancer therapy*

1. INTRODUCTION

Tumor tissues are highly heterogeneous, and tumor cells exist in a complicated network of tumor microenvironment (TME) composed of various immune cells and stromal cells such as endothelial cells, pericytes, fibroblasts, macrophages, T cells, etc.[1−5] Immunosuppression and hypoxia are the key features of the TME and are also crucial factors for the efficacy of cancer therapy and tumor metastasis.[6−8] Immunotherapy with immune checkpoint inhibitors (ICIs) has been developed as an effective method to treat cancers, which obtains encouraging therapeutic outcomes and improves patients' survival in certain types of cancers.[9] However, the overall response rate for patients receiving ICI treatment ranged from 15 to 60% in many solid tumor types.[10] Thus, how to enhance the overall response rate of ICIs in the tumors with tolerance to ICIs is an important issue for cancer immunotherapy and clinical practice. Increasing evidence indicates that tumor immune microenvironment and inherent antitumor immunity are crucial for ICIs' efficacy.[11]

Recently, it has been found that immunogenic cell death (ICD) induced primarily in cancer cells with various therapeutic modalities provides a good strategy to initiate systemic antitumor immunity and improve the efficacy of ICIs for immunotherapy.[12−14] ICD enhances antitumor immune responses by eliciting a range of tumor antigens and damage-associated molecular patterns (DAMPs), such as the exposure of calreticulin (CRT) onto the surface of cancer cells and the release of high-mobility group box 1 (HMGB1) and adenosine

Received: March 31, 2023
Revised: April 24, 2023
Accepted: April 26, 2023
Published: May 9, 2023

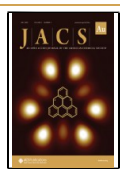

https://doi.org/10.1021/jacsau.3c00156
JACS Au 2023, 3, 1507−1520

Scheme 1. Antitumor Diagram Involved in This Work through Augmented Immunogenic Cell Death and Antitumor Immunity Mediated by Sonodynamic Therapy and Ferroptosis Inducer

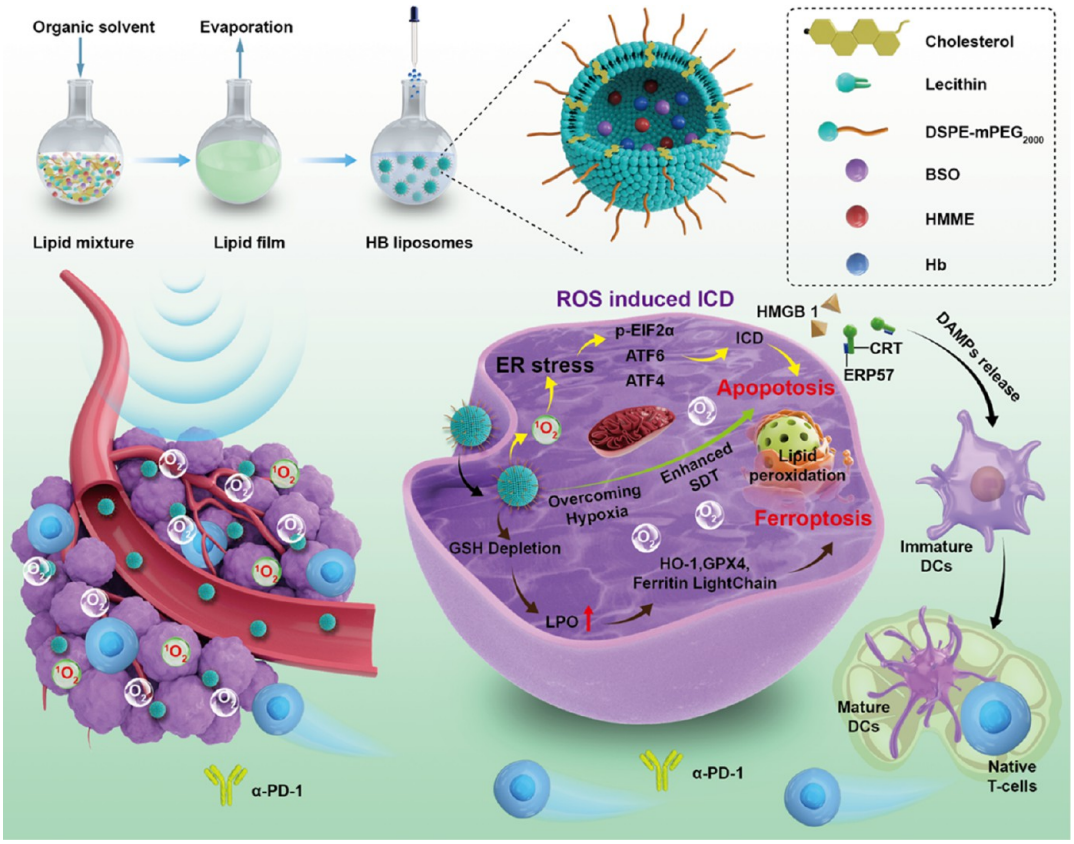

triphosphate (ATP) from dying cancer cells. DAMPs could activate the intrinsic antitumor immune system through the induction of dendritic cell (DC) maturation, recruitment of phagocytes, enhanced infiltration of cytotoxic T cells, and proinflammatory cytokine releases.[15,16] To date, the majority of ICD inductions have primarily resulted from apoptotic cell death initiated by various therapeutic modalities, such as chemotherapy, photothermal therapy, photodynamic therapy, and sonodynamic therapy (SDT); however, tumor resistance to the apoptotic pathway considerably impeded the efficient induction of ICD during cancer treatment and subsequent activation of adaptive immunity.[17] As apoptosis is the most common pathway for regulated tumor-cell death, exploring novel non-apoptotic cell death pathways with high immunogenicity is crucial to alter tumor immune microenvironment and facilitate antitumor function of ICIs. Ferroptosis is a novel type of non-apoptotic regulated cell death characterized by the depletion of glutathione, accumulation of lipid peroxides (LPO), and further induction of oxidative stress. Furthermore, it has been proven that DAMPs could be elicited in cancer cells during ferroptosis to participate in the modulation of tumor immune microenvironment.[18−21] Although there are conflicting findings about the relationship between ferroptosis and antitumor immunity, which might be dependent on tumor types or classes of ferroptosis inducers,[22,23] multiple lines of evidence were shown that cancer cell death resulting from ferroptosis, especially early ferroptosis, could enhance antitumor immunity and efficacy of immunotherapy.[24,25]

Ultrasound (US)-mediated cancer therapy is a localized therapeutic modality for tumor treatment with good penetration of tissue and the ability to effective ICD induction to further activate tumor-specific immune responses.[26] SDT, a type of reactive oxygen species (ROS)-mediated cancer therapy, utilizes harmless US to initiate the generation of ROS to kill tumor cells.[27−29] The ROS, in turn, could also trigger endoplasmic reticulum (ER) stress that elicits the production of DAMP signals and further leads to ICD.[30,31] Therefore, SDT is another therapeutic modality for efficient ICD induction through ROS-initiated ER stress and could also potentially stimulate antitumor immunity.

Compared with traditional photodynamic therapy, SDT exhibits a higher tissue penetration, rendering it a promising and potent therapeutic modality for cancer treatment. However, since SDT requires more oxygen to generate ROS, rapid oxygen consumption can aggravate the hypoxia state inside the tumors, which might dampen the therapeutic effect of SDT. Thus, enhancing supplement of oxygen into tumor mass is a reasonable strategy to improve the therapeutic efficacy of SDT. Currently, various strategies have been designed to alleviate tumor hypoxia, such as introduction of microbubbles containing oxygen, in situ O_2 generation by metals, or catalase reacting with intratumoral H_2O_2 and hemoglobin (Hb).[32−35]

Notably, cancer immunotherapies that reverse tumor immunosuppressive microenvironment or stimulate the host immune system are changing the therapeutic landscape for multiple malignancies. In terms of immune response modulation under SDT, it has been reported that SDT could improve the efficacy of immunotherapy through induction of ROS or rapid consumption of glutathione.[36−38]

In the present study, we aimed to establish a combined therapeutic strategy integrated SDT with ferroptosis inducer

https://doi.org/10.1021/jacsau.3c00156
JACS Au 2023, 3, 1507−1520

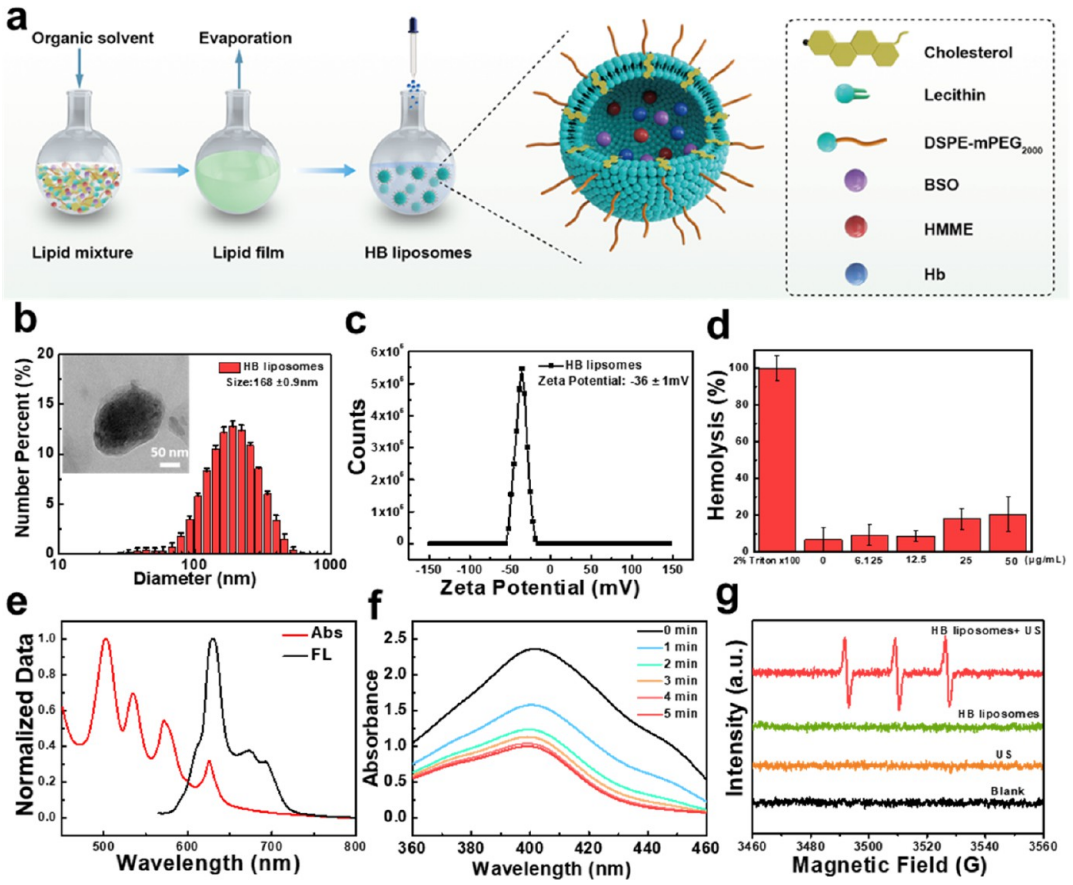

Figure 1. (a) Schematic illustration for the synthetic procedure of HB liposomes. (b) Size distribution of HB liposomes analyzed by dynamic light scattering and TEM images. (c) Zeta potential analysis of HB liposomes. (d) Hemolysis assay of HB liposomes. (e) Normalized absorption spectra and fluorescence spectra of HB liposomes. (f) Time-dependent DPBF absorption spectra in the presence of HB liposomes under US irradiation for different durations (g) ESR spectra for $^1O_2$ generation under various treatments (PBS, US, HB liposomes, and HB liposomes plus US) with TEMP as a trapping agent.

and oxygen supplement to induce ICD and modulate the tumor immune microenvironment (Scheme 1). This was achieved using BSO, a constructed GSH synthesis inhibitor, Hb, and sonosensitizers (HMME) co-loaded into nanoliposomes as the nanosonosensitizers (termed HB liposomes). After intravenous administration, HB liposomes accumulated at the tumor site due to the EPR effect and could exert a sonodynamic effect on primary tumors to produce ROS under the treatment of US. The Hb is then able to provide oxygen at the hypoxic site of tumors, which enhances tumor oxygenation and improves the effectiveness of SDT. In addition, the triggered ER stress by ROS can activate ICD and result in the release of DAMPs to further promote the maturation of DC, increase the infiltration of the cytotoxic T lymphocytes, and remodel the TME. Similarly, enhanced tumor cell death by ferroptosis-inducer BSO also synergistically induces the release of DAMPs and further regulates the TME. In addition, this nanotherapeutic system combined with PD-1 checkpoint blockade achieves a superior synergistic anticancer effect. Therefore, the objective of this study is to use SDT combined with the ferroptosis inducer and supply of oxygen to amplify the ICD, eventually enhancing tumor suppression and modulating the TME. The strategy proposed in this work provides a novel and alternative approach for cancer therapy through amplification of tumor cell ICD and enhancement of antitumor immunity.

2. RESULTS AND DISCUSSION

Liposomes were used as nanoplatforms to co-encapsulate three hydrophobic molecules: the sonosensitizer HMME, glutathione synthesis inhibitor L-buthionine-sulfoximine (BSO), and oxygen supplier Hb, via the typical reverse evaporation method (designated as HB liposomes). The preparation process for HB liposomes is illustrated in Figure 1a. TEM imaging and dynamic light scattering indicated that the average hydrodynamic size of HB liposomes was ∼168 nm (Figure 1b), and the zeta potential analysis showed high negative zeta potential (−36 mV), which is conducive to maintain stability of nanoparticles within the bloodstream (Figure 1c). As demonstrated in Figure S1, the HB liposomes exhibited high dispersity in various solvents, including H_2O, PBS, and RPMI 1640 with 10% fetal bovine serum. Overall, the nanoscale size and negative zeta potential facilitate the HB liposomes to penetrate into tumor tissues via the EPR effect.

Next, the hemolysis assay was conducted under various concentrations of HB liposomes. Figure 1d reveals that no obvious hemolysis phenomenon was observed, which implicates that the HB liposomes exhibit excellent biosafety and biocompatibility. As indicated in Figures 1e and S2, UV−vis spectrum analysis showed that HB liposomes exhibited four characteristic absorption peaks between 450 and 650 nm, which is similar to free HMME, indicating that HB liposomes still retain their the nanosonosensitizer ability of HMME. The

https://doi.org/10.1021/jacsau.3c00156
JACS Au 2023, 3, 1507−1520

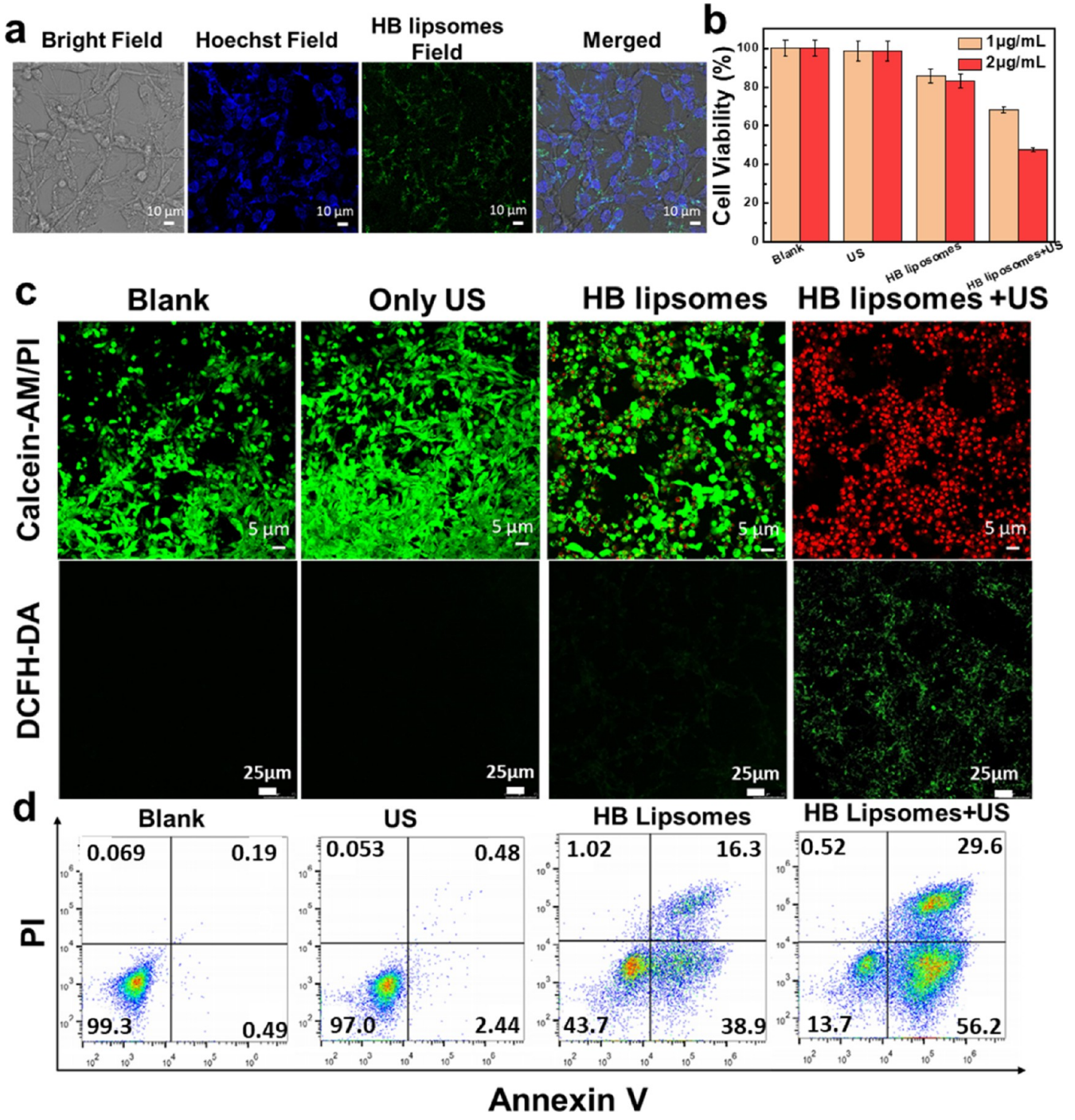

Figure 2. (a) CLSM images of internalization of HB liposomes in Colon 26 cells. (b) Cell viability of Colon 26 cells under various treatments with or without US (3.0 MHz; 1.5 W cm^{-2}; 50% duty cycle) for 1 min. (c) Live/dead cell staining (upper) and the intracellular ROS level (lower) of Colon 26 cells treated with HB liposomes under various conditions. (d) Cell apoptosis assessment with Annexin V/PI staining by flow cytometry after various treatments.

loading efficiency of HMME, which is essential for effective anticancer therapy, was determined to be 89% as shown in Figure S3. Nanosonosensitizer-assisted SDT typically induces the production of ROS, such as singlet oxygen ($^1O_2$), which kills cancer cells. To monitor the ROS during the SDT process, the ROS probe 1,3-diphenylisobenzofuran (DPBF) and electron spin resonance (ESR) were employed to analyze ROS generation. As indicated in Figure 1f, the characteristic absorption peak at 400 nm significantly decreased with increasing US irradiation time, which suggests that extensive ROS was produced in the solution. In addition, we observed obvious and strong ESR characteristic peaks of $^1O_2$ species for HB liposomes upon US irradiation, whereas no evident peak was observed in other groups (Figure 1g). Taken together, the results demonstrate that the constructed nanocomposites display expected characteristics such as excellent biosafety, great capability of singlet oxygen production, and good nanosonosenitizer property.

To further evaluate internalization of HB liposomes by cancer cells, the intracellular green fluorescence by CLSM

https://doi.org/10.1021/jacsau.3c00156
JACS Au 2023, 3, 1507−1520

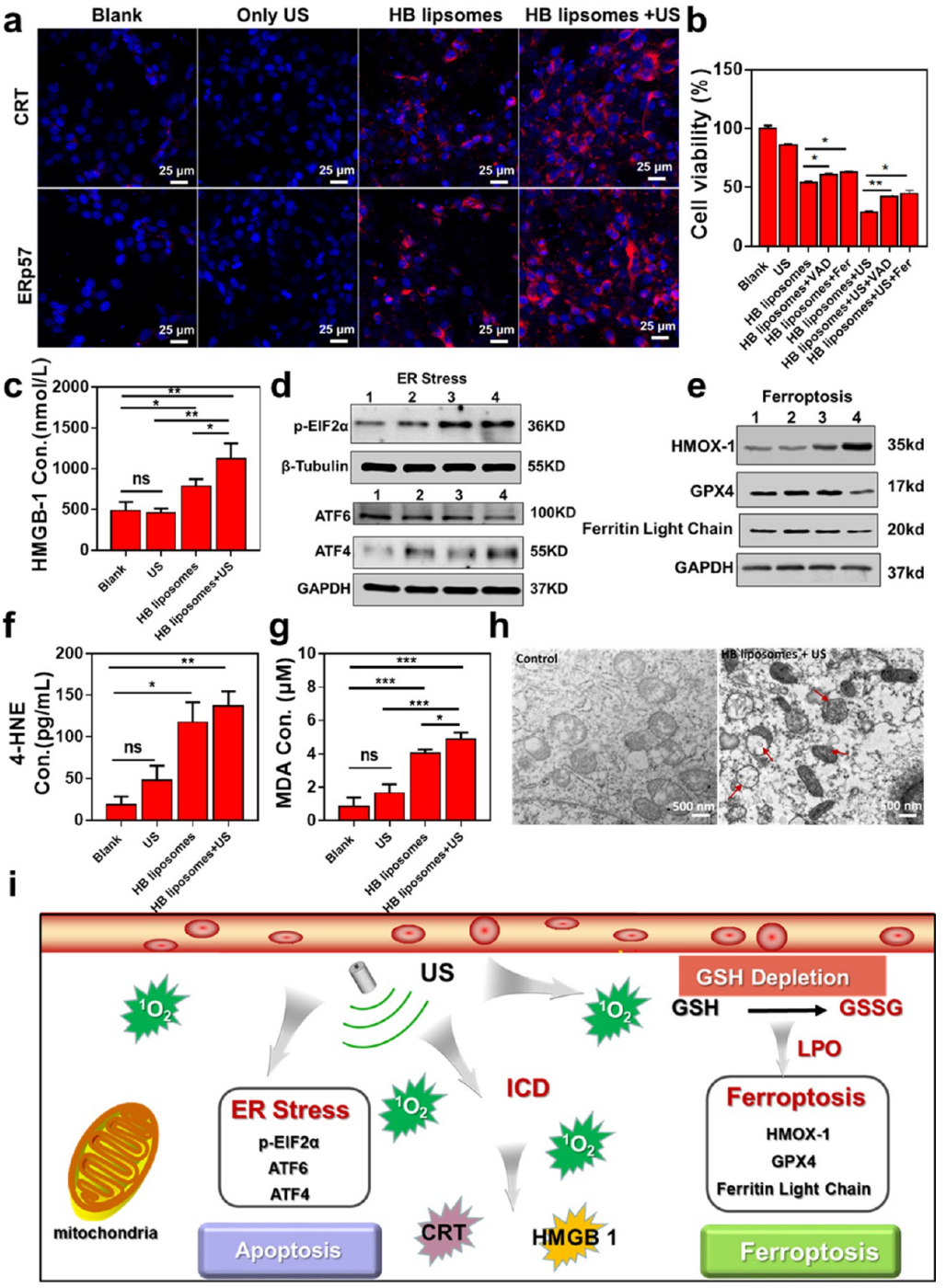

Figure 3. (a) Immunofluorescence staining for cell surface CRT and ERp57 after various treatments. (b) Cell viability of Colon 26 cells under various treatments. (c) Release of HMGB-1 from Colon 26 cells after different treatments (n = 3). (d) Western blotting analysis of the ER stress pathway in Colon 26 cells after various treatments [(1) Blank; (2) US; (3) HB liposomes; (4) HB liposomes + US]. (e) Western blotting analysis of the ferroptosis pathway in Colon 26 cells after various treatments [(1) Blank; (2) US; (3) HB liposomes; (4) HB liposomes + US]. (f) Relative 4-HNE content from Colon 26 cells after various treatments (n = 3). (g) Relative MDA content from Colon 26 cells after various treatments (n = 3). (h) Bio-TEM images of glutaraldehyde-fixed Colon 26 cells pretreated with HB liposomes plus US. ***P < 0.001. (h) Schematic illustration of the proposed molecular mechanism for Colon 26 cells based on ferroptosis/apoptosis induced by SDT.

images suggested efficient internalization of HB liposomes by Colon 26 cells after 24 h incubation (Figure 2a). Next, we investigated the cytotoxic effect of SDT on Colon 26 cells by the MTT assay. As shown in Figure 2b, treatment with HB liposomes plus US could significantly inhibit the cell viability in a dose-dependent manner. Moreover, calcein acetoxymethyl ester (calcein-AM) and propidium iodide (PI) co-staining assays were further conducted to confirm the cytotoxic activity of HB liposomes plus US. The fluorescence images revealed no distinct differences between the blank and US only groups, in which most of the cells showed green colorization of calcein-AM, implicating intact live cells in these two groups. However, the treatment with HB liposomes plus US resulted in obvious red staining of PI in most of the Colon 26 cells, implying cell

https://doi.org/10.1021/jacsau.3c00156
JACS Au 2023, 3, 1507−1520

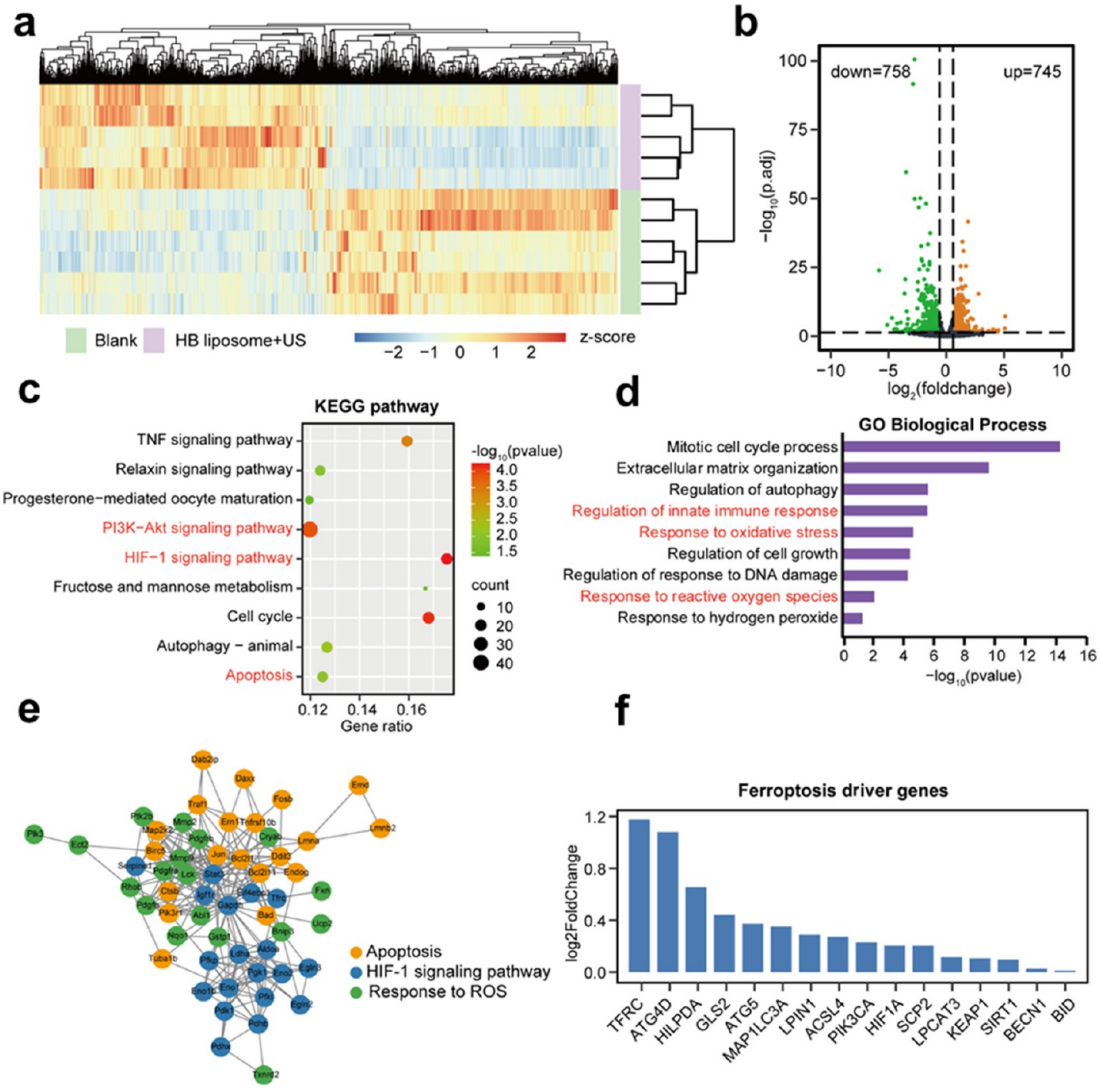

Figure 4. (a) Heat map showing the differentially expressed genes in Colon 26 cells after treatments. (b) Volcano plot indicating the upregulated and downregulated genes after the double treatment. (c) KEGG pathway enrichment analysis after treatments. (d) GO enrichment analysis for the biological processes differentially regulated after treatments. (e) Protein−protein interaction network of apoptosis, the HIF-1 signaling pathway, and response to ROS in double treatment group. (f) Driver gene-involved ferroptosis induction after the double treatment.

death (Figure 2c). HB liposomes alone also slightly induced cell death with PI staining, which might be ascribed to the ferroptosis inducer BSO (Figure 2c). Subsequently, ROS generation was analyzed with the DCFH-DA probe. As shown in Figure 2c, HB liposomes plus US markedly promoted the production of ROS, but there was no obvious ROS signal in other groups. Since ROS could induce cell apoptosis, flow cytometry for apoptosis detection with Annexin V/PI staining was carried out after various treatments as shown in Figure 2d. The data disclosed that HB liposomes plus US remarkably increased early (29.6%) and late (56.2%) apoptosis when compared with other groups. US alone did not result in obvious cell apoptosis, whereas HB liposomes alone also significantly induced early (16.3%) and late (38.9%) apoptosis possibly owing to the increase of the intracellular ROS level that resulted from the GSH depletion.

To evaluate the ICD on tumor cells after SDT, we first examined the exposure of CRT/ERp57 and the release of HMGB1, all of which are well-known indicators of ICD. As shown in Figure 3a, treatment with HB liposomes plus US could induce more surface exposure of CRT and ERp57 in Colon 26 cells compared with that of HB liposomes alone. No obvious surface staining of CRT and ERp57 was identified in the control groups of US only and blank. In addition, the double treatment (HB liposomes plus US) caused increased release of HMGB1 from Colon 26 cancer cells when compared with other three control groups (Figure 3c). Thus, in vitro data suggested that SDT based on HMME in HB liposomes could enhance ICD induction in cancer cells and potentially could initiate stronger antitumor responses in vivo. Given that ROS is associated with the activation of stress responses, we thus investigated whether HB liposomes plus US could induce ER stress in Colon 26 cells. As shown in Figure 3d, phosphorylation of eukaryotic initiation factor 2α (eIF2α), a characteristic indicator of the ER stress response, was significantly increased after the double treatment and HB-liposome treatment, indicating that both treatments could induce ER stress and HB liposomes alone might also produce some ROS due to BSO's ability to inhibit the synthesis of GSH. Upon initiation of ER stress, transcription factor-4

https://doi.org/10.1021/jacsau.3c00156
JACS Au 2023, 3, 1507−1520

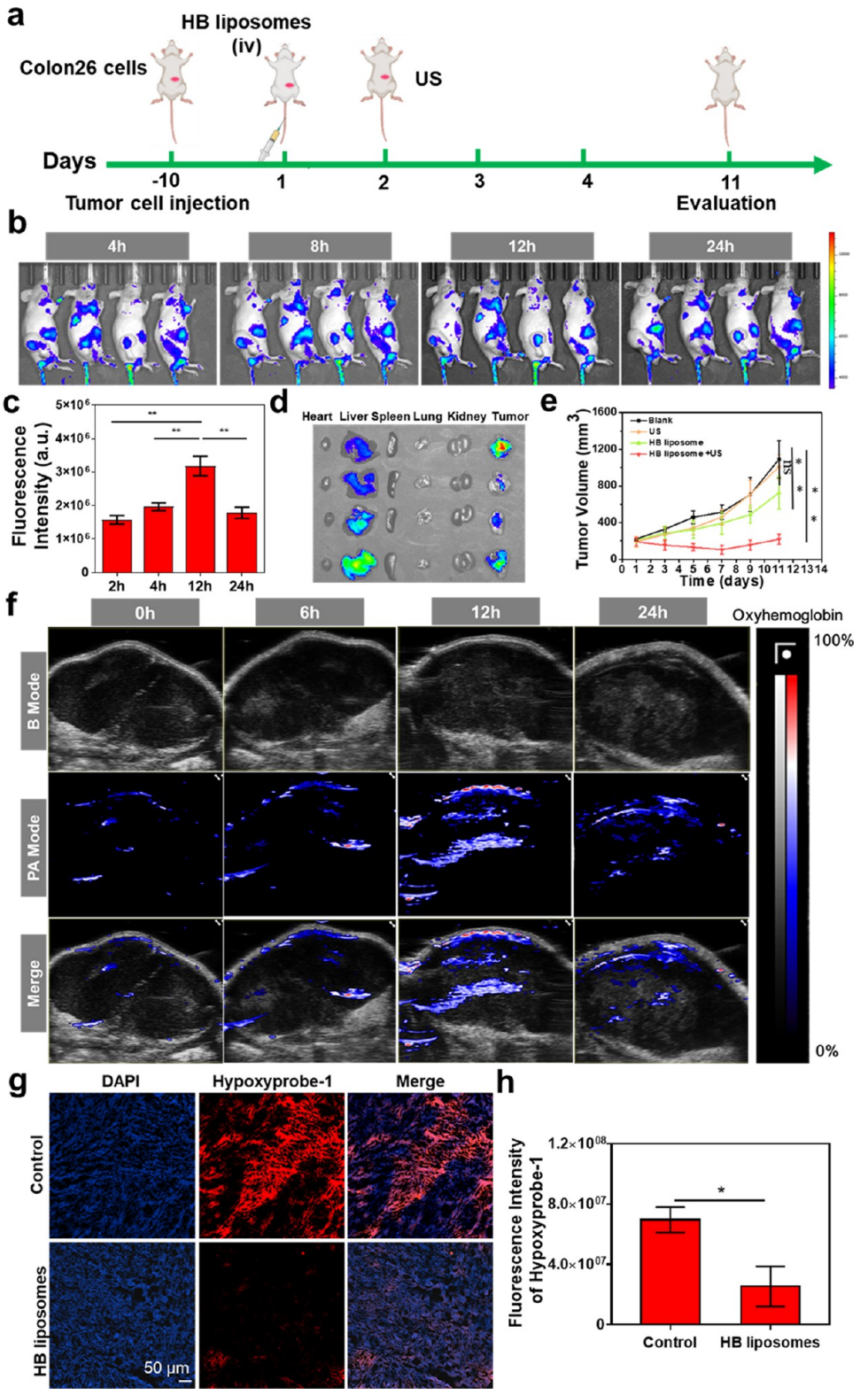

Figure 5. Antitumor efficacy of HB liposomes plus US in tumor-bearing mice. (a) Schematic illustration for the therapeutic schedule. (b) In vivo imaging of Cy5-labeled HB liposomes in Colon 26 tumor-bearing mice at different time points (n = 4). (c) Quantitative analysis of the fluorescence intensity at different time points. (d) Biodistribution of Cy5-modified HB liposomes in major organs and tumor excised from the mice. (e) Tumor growth curves after various treatments (n = 5). (f) PAI of tumors at different time points after the injection of HB liposomes. (g) Hypoxia evaluation by the immunofluorescent staining after hypoxyprobe-1 treatment. (h) Quantitative analysis of the hypoxia level after treatment with hypoxyprobe-1.*P < 0.05, **P < 0.05, and ***P < 0.001.

(ATF4) is activated and upregulated by the excess ROS through the PERK/eIF2α/ATF4 pathway. Our data revealed that ATF4 was increased after the double treatment of HB liposomes plus US (Figure 3d). In addition, ATF6, an ER

https://doi.org/10.1021/jacsau.3c00156
JACS Au 2023, 3, 1507−1520

transmembrane transcription factor, is activated by the ER stress/unfolded protein response, where 90 kDa ATF6 is converted to a 50 kDa protein.[39] Indeed, the double treatment resulted in the obvious reduction of 90 kDa ATF6, implying strong ER stress in Colon 26 cells. Since BSO is an inhibitor of GSH synthesis and abundant ROS could accelerate the depletion of GSH, the reduction in intracellular GSH content was further assessed by the reduced GSH assay kit. Notably (Figure S4). HB liposomes alone and the double treatment (HB liposomes plus US) could obviously lower GSH content compared with that of blank and US alone after incubation for 25 min. The depletion of GSH and excessive ROS were reported to lead to glutathione peroxidase 4 (GPX4) inactivation and thus could cause subsequent accumulation of lipid peroxidation and ferroptosis. In the presence of HB liposomes plus US, intracellular GPX4 expression was remarkably decreased (Figure 3e), implying that the HB liposomes plus US overwhelmed the antioxidative defense system in the cancer cells. However, HB liposomes alone did not obviously affect the expression of GPX4, indicating that BSO alone in HB liposomes is not enough to impact GPX4 and combinational therapy is necessary to maximize the ferroptosis induction. Meanwhile, another two ferroptosis markers ferritin light chain (FTL), and heme oxygenase-1 (HMOX1) were also evaluated after various treatments. FTL as a component of ferritin for iron ions storage was significantly decreased after the double treatment; in contrast, HMOX1, catalyzing the degradation of HMME to increase iron ions, was markedly increased after double treatment, and HB liposomes alone also slightly induced the increase of HMOX1. The expression changes of both proteins indicate that ferroptosis is induced and augmented after treatment with the constructed nanocomposite plus US compared with that of HB liposomes alone which contain ferroptosis inducer BSO but do not receive US irradiation (Figure 3e).

Next, malondialdehyde (MDA) and 4-hydroxynonenal (4-HNE) were measured after various treatments. Both molecules are reactive aldehydes and increased during ferroptosis. They could also reflect the level of intracellular lipid peroxidation. As shown in Figure 3f,g, HB liposomes and HB liposomes plus US treatment can significantly elevate the levels of MDA and 4-HNE, and the double treatment could maximize the increase for both molecules. Morphological examination of mitochondria in Colon 26 cells treated with HB liposomes plus US exhibited prototypical ferroptotic characteristics, such as impaired mitochondrial outer membrane, reduced mitochondrial volume, and lost mitochondrial ridge (Figure 3h). As shown in Figure 3b, the presence of ferroptosis inhibitor Fer-1 can obviously reverse the viability of cells treated with HB liposomes or HB liposomes plus US in both groups. In addition, the addition of apoptosis inhibitor VAD can also partially reverse the viability of cells treated with HB liposomes or HB liposomes plus US. These results demonstrate the participation of both apoptosis and ferroptosis in HB liposome-mediated therapy. In summary, the potential antitumor mechanism of HB liposomes is shown in Figure 3i. When exposed to US, the HB liposomes containing the sonosensitizer HMME can generate ROS to trigger ER stress that elicits the DAMP signal release and further induces ICD. In addition, ROS could cause irreversible damages to proteins and other macromolecules to induce apoptosis. However, the SDT-triggered cellular ROS cytotoxicity may be attenuated by the intracellular antioxidant system. BSO as a ferroptosis inducer can block the synthesis of superoxide scavenger GSH. Thus, BSO in HB liposomes could facilitate to maintain the ROS level inside the tumor mass and further stabilize the cytotoxic activity of ROS. Notably, ROS induced from treatment with HB liposomes plus US could result in ER stress and mitochondrial dysfunction in tumor cells, which subsequently cause tumor cell apoptosis, ICD, and the release of DAMPs.

To widely explore the whole landscape of gene expression pattern in Colon 26 cells after treatment with the sonodynamic nanosystem in cancer cells, RNAseq analysis was conducted to analyze the differential gene expression after treatment. There were 1503 differentially expressed genes between the double treatment group (HB liposomes plus US) and the blank group ($FC \geq 1.5$, $p < 0.05$), of which 745 were upregulated and 758 were downregulated (Figure 4a,b). KEGG pathway analysis revealed that signaling pathways for PI3K−Akt and HIF-1, apoptosis and cell cycle were enriched after the double treatment, all of which were highly associated with the observed cell death (Figure 4c). The analysis of GO biological process indicated that a series of important biological processes correlated to cell growth inhibition and oxidative stress were enriched after the double treatment such as the mitotic cell cycle process, regulation of innate immune response, and cell growth, response to oxidative stress and ROS (Figure 4d). All of these processes are highly connected to the ingredients of nanocomposite and ultrasonic irradiation. Indeed, strong interactions between genes involved in apoptosis, hypoxia factors, and response to ROS were observed (Figure 4e). We also noticed that autophagy was enriched in analysis of the KEGG pathway and GO analysis. It has been demonstrated that autophagy is directly correlated to ferroptosis.[40] Since we demonstrate that ferroptosis is induced after the double treatment, we further specifically analyzed the genes driving ferroptosis from RNA-seq data. As a result, a panel of ferroptosis driver genes showed an upward trend in overall expression after the double treatment including TFRC, ATG4D, GLS2, ATG5, ASCL4, LPCAT3, BECN1, BID, and so on, which indicated that ferroptosis was highly involved in the process of tumor growth inhibition (Figure 4f). Collectively, the RNA-seq data disclose that HB liposomes plus ultrasonic irradiation could inhibit cell growth through ROS generation, apoptosis, and ferroptosis.

Given its excellent in vitro therapeutic performance, HB liposomes were further evaluated for their in vivo anticancer activity (Figure 5a). First, tumor accumulation and biodistribution of HB liposomes were evaluated by in vivo fluorescence imaging. Cy5-modified HB liposomes were administered intravenously to Colon 26 tumor-bearing mice and the fluorescence signals from various time points were recorded. As shown in Figure 5b,c, the HB liposomes showed the strongest tumor accumulation at 12 h post-injection; and the fluorescence signal gradually faded out at 24 h, indicating that HB liposomes is suitable for local ultrasonic irradiation in tumor sites. For detailed tissue distribution of HB liposomes, the mice were sacrificed to harvest major organs and tumor tissues 24 h after liposome injection for ex vivo fluorescence imaging, showing a higher tumor accumulation of HB liposomes compared with other organs except livers which are responsible for liposome clearance (Figure 5d).

Meanwhile, O_2 release by Hb at hypoxic tumor sites may contribute to improved tumor oxygenation and subsequently enhance SDT efficacy. To verify this, we monitored the tumor

https://doi.org/10.1021/jacsau.3c00156
JACS Au 2023, 3, 1507−1520

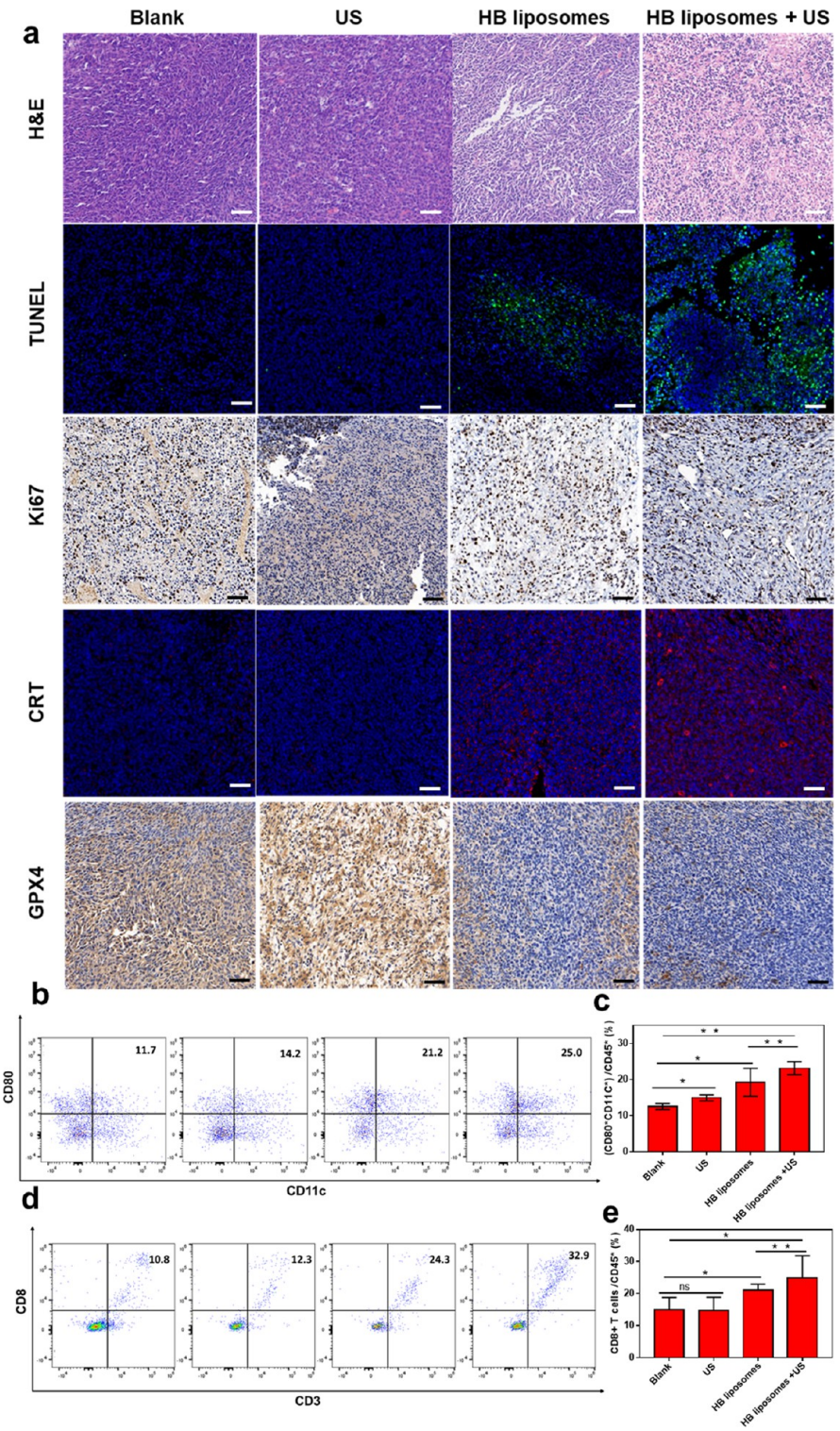

Figure 6. (a) H&E staining and immunohistochemical staining for the TUNEL assay, CRT exposure, and the expression Ki67 and GPX4. Scale bars: 50 μm. (b) Flow cytometric and (c) quantitative analyses of mature DCs ($CD45^+CD80^+$ $CD11c^+$) in tumors after various treatments. (d) Flow cytometric and (e) quantitative analyses of $CD8^+$ T cells ($CD45^+CD3^+CD8^+$) in tumors after various treatments (n = 3). ***P < 0.001.

oxygenation by photoacoustic imaging (PAI) of Hb and oxyhemoglobin. As shown in Figure 5f, PAI disclosed that HB liposomes significantly improved the oxygen concentration (sO_2) in tumor tissues over time, reaching a peak within 12 h and subsequently decreasing, which seems to be in agreement with the timeline of tumor imaging after Cy5-modified HB liposomes. Therefore, liposomes encapsulated with Hb are beneficial to improve intratumoral oxygenation and enhance the efficacy of SDT. Meanwhile, as shown in Figure 5g,h, we further analyzed the extent of hypoxia in tumors by pimonidazole hydrochloride (hypoxyprobe-1), to determine whether HB liposomes treatment could improve the hypoxia of tumor tissues. The data indicated that the untreated control tumors exhibited strong hypoxia signals while the hypoxia level

https://doi.org/10.1021/jacsau.3c00156
JACS Au 2023, 3, 1507−1520

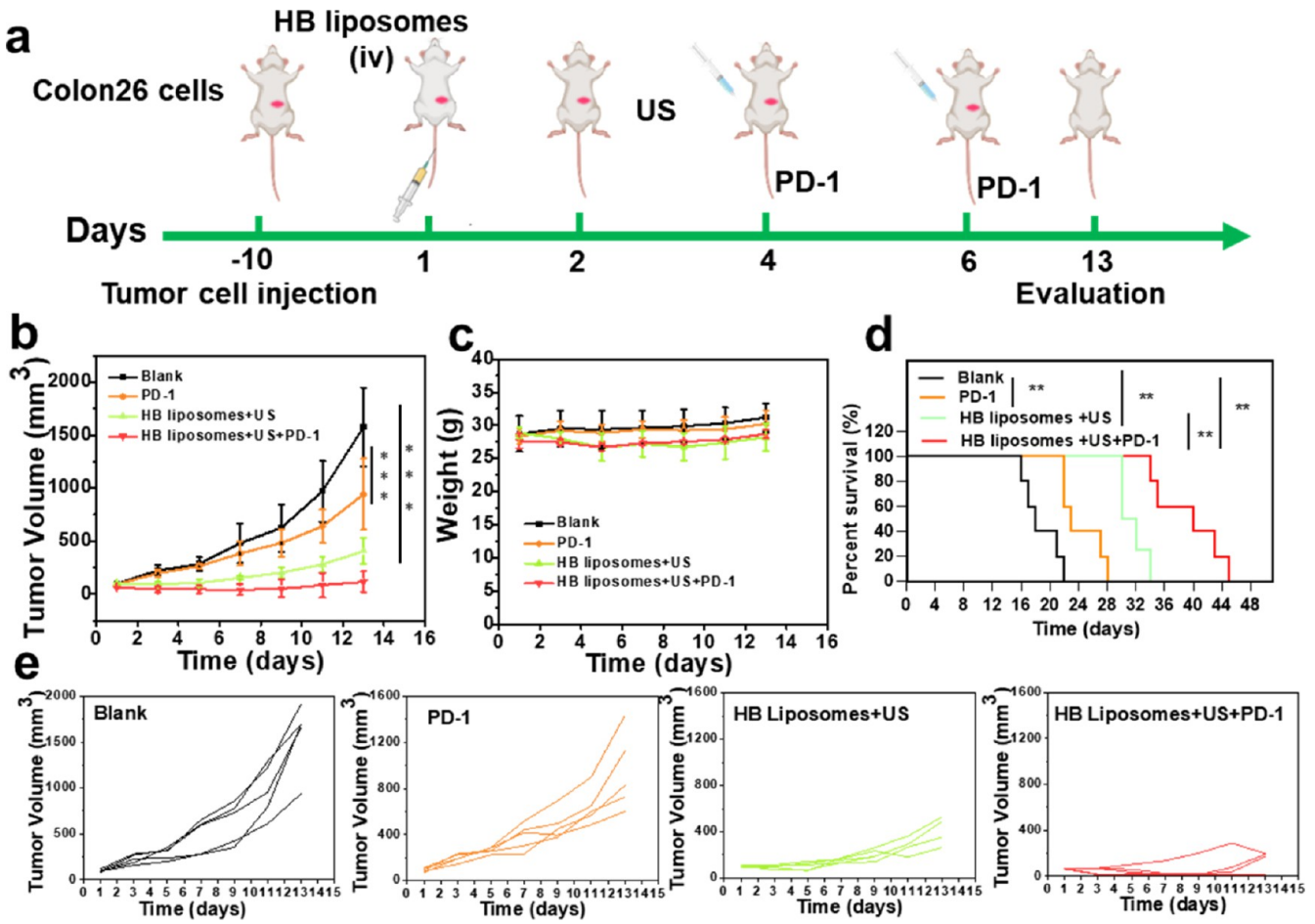

Figure 7. (a) Schematic therapeutic schedule of the HB liposome sonodynamic system combined with PD-1 antibody. (b) Individual tumor growth curves for each mouse in four groups (n = 5). (c) Body weight during the whole treatment and (d) survival curves for tumor-bearing mice after different treatments. (e) Tumor growth curves in four groups with different treatments (n = 5).

was significantly lowered in HB liposomes-treated tumors suggesting that HB liposomes could relieve hypoxia in the solid tumors and could reoxygenate the hypoxic tumor environment.

Subsequently, in vivo antitumor study was performed with Colon 26 tumor-bearing mice. Mice were randomly assigned to four groups: Blank (PBS) group, US irradiation alone group (3.0 MHz; 1.5 W cm^{-2}; 50% duty cycle; 5 min), HB liposomes alone group, and the double treatment group (HB liposomes plus US irradiation). As shown in Figure 5e and Figure S5, the tumors from two control groups (blank and US irradiation alone) grew rapidly over the treatment period. The tumors receiving the treatments with HB liposomes alone and the double treatment (HB liposome plus US irradiation) were suppressed significantly when compared with blank and US alone. The double treatment with HB liposomes plus US irradiation showed maximal tumor growth inhibition across four groups. These results confirmed that HB liposomes loaded with HMME could produce potent antitumor effects upon US irradiation. Moreover, only minor insignificant fluctuations in mice body weight were observed across all groups during 11 days after liposomes administration, indicating that no severe acute toxicity was generated for HB liposomes and US irradiation in tumor-bearing mice (Figure S6). In addition, blood parameter analysis and histological analysis of the major organs were performed to investigate the biosafety of HB liposomes and US. As shown in Figures S7 and S8, no systemic toxicity was observed according to various blood parameters. Hematoxylin and eosin (H&E) staining for the major organs with various treatments did not suggest detectable inflammation or damage, implying that no obvious in vivo toxicities were caused by SDT (Figure S9). These results further demonstrate that the treatment with HB liposomes plus US possesses good biocompatibility and holds great promise for clinical translation.

To assess the effects of HB liposomes plus US on tumor apoptosis, proliferation, and ferroptosis, tumor sections in each group were first subjected to H&E staining, Ki67, and apoptotic analysis with TUNEL staining. As shown in Figure 6a, H&E staining revealed massive tumor cell death after the double treatment, and HB liposomes alone also resulted in significant cell death; no obvious cell death was observed in other control groups. TUNEL assays indicated similar results with H&E staining, showing that the HB liposomes plus US induced extensive cell apoptosis, and apoptotic cells were slightly increased in the group of HB liposomes alone (Figure 6a). In contrast with apoptosis, the Ki67 level more significantly decreased in the groups of HB liposomes alone and HB liposomes plus US than that of other two control groups, and the double treatment showed minimal level of Ki67-positive staining across all groups. GPX4 as an indicator was significantly reduced in two groups containing HB liposomes, and the double treatment further suppressed the

https://doi.org/10.1021/jacsau.3c00156
JACS Au 2023, 3, 1507−1520

expression of GPX4. Since ICD could be elicited by biological processes related to apoptosis and ferroptosis, the exposure of CRT protein as a marked event for ICD was assessed by immunostaining. The data suggested that ICD was induced by HB liposomes alone and the double treatment, but the latter resulted in more exposure of CRT onto the cancer cell surface (Figure 6a).

Since ICD in tumor tissues is highly associated with the modulation of immune microenvironment, we next evaluated whether SDT based on HB liposomes could enhance antitumor immunity. We analyzed the immune cells in tumor tissues after various treatments. As indicated in Figure 6b,c, mature DCs ($CD11c^+CD80^+$) in tumor tissues were significantly increased after treatment with HB liposomes plus US (25%) when compared with that of HB liposomes alone (21.2%), US alone (14.2%), and blank (11.7%). DCs as a kind of antigen-presenting cells could process tumor antigens and present the processed antigens to T cells.[15] It has been demonstrated that molecules of DAMPs released or exposed from immunogenic dead cells (CRT or ATP) could induce DC maturation and further activate T cells inside tumor tissues, thereby enhancing antitumor immunity. Thus, infiltrated T cells were further assessed by flow cytometry. The data suggested that more $CD8^+$ cytotoxic T cells (32.9%) were found in tumors that received the double treatment compared with HB liposomes alone (24.3%), US alone (12.3%), and blank (10.8%) (Figure 6d,e). We did not observe significant changes in other immune cells such as CD4 T cell, macrophages, and NK cells (data not shown). Since the double treatment of HB liposomes plus US could induce most mature DCs and infiltrated $CD8^+$ T cells in tumor mass, this nanosystem integrating nanoparticles, ferroptosis inducer (BSO), oxygen supplier (Hb), and sonosensitizer (HMME) could not only result in apoptosis/ferroptosis of tumor cells but also modulate tumor immune microenvironment after being administered into tumor-bearing mice and irradiated with local ultrasonic treatment.

Immunotherapy with ICIs such as PD-1 antibody and CTLA4 antibody has revolutionized the cancer therapeutics and significantly prolonged the survival rate in patients with certain cancers.[41] Among the parameters affecting ICI response, tumor-infiltrating immune cells, especially cytotoxic T cells ($CD8^+$), are one of the determinants for ICI efficiency.[42] Encouraged by the increased $CD8^+$ T cell infiltration after the treatment with HB liposomes plus US (Figure 6d), we next evaluated the antitumor efficiency of PD-1 antibody in HB liposomes/US-treated tumor-bearing mice (Figure 7a). Colon 26 tumor-bearing mice were assigned to four groups for various treatments as illustrated schedule in Figure 7a (1, Blank; 2,PD-1 alone; 3, HB liposomes plus US; and 4, HB liposomes/US plus PD-1). As a result, two doses of PD-1 injection (250 μg/mouse) just showed a weak antitumor effect (Figure 7b,e). By contrast, double treatments with HB liposomes plus US obtained a potent antitumor effect, which is consistent with previous study in Figure 5e. Notably, triple treatment with HB liposomes/US plus PD-1 antibody inhibited tumor growth more significantly than double treatments (Figure 7b,e), indicating that disruption of the interaction between PD-1/PD-L1 axis markedly enhances T cell antitumor function, which corresponds with the increase $CD8^+$ T cell infiltration after the treatment of HB liposomes plus US (Figure 6d). Meanwhile, only minor insignificant fluctuations in body weight were observed across all groups (Figure 7c), implicating the good biosafety for this therapeutic regimen. In addition, triple treatments with HB liposomes/US plus PD-1 most significantly prolonged the survival of tumor-bearing mice when compared with other three control groups although the double treatment already extended the mice survival (Figure 7d). Together, these results further demonstrate that HB liposomes plus US could not only directly suppress tumor growth but also spontaneously induce $CD8^+$ T cell infiltration into tumor sites, which creates a precondition for combination therapy with immunotherapy. Indeed, immune checkpoint blockade PD-1 antibody could further synergistically delay tumor growth.

3. CONCLUSIONS

In summary, a distinct liposomal nanocomposite was successfully developed for enhanced SDT. In the constructed nanosystem, HB liposomes loaded with an inhibitor of GSH synthesis BSO led to the depletion of GSH and the increased production of lipid peroxidation, which synergistically trigger the ferroptosis of tumor cells. Furthermore, HMME entrapped into HB liposomes renders SDT feasible, causing the production of ROS which, in turn, augments apoptosis and ferroptosis of tumor cells. On the other hand, the Hb proteins encapsulated into HB liposomes could provide more oxygen to increase the efficacy of SDT. Both cell deaths initiate the induction of ICD and release of DAMPs, thereby promoting DC maturation and $CD8^+$ T cell infiltration into tumor mass. Addition of PD-1 antibody to this nano−sono modality further amplifies the inhibitory effect on tumor growth. Collectively, this distinct liposomal nanosystem combined with ultrasonic irradiation (SDT) not only causes massive tumor cell death (apoptosis and ferroptosis) but also modulates the TME with favorable antitumor immunity, which creates the opportunity for immune checkpoint blockade to further improve the efficacy and response rate of immunotherapy.

4. METHODS

4.1. Analysis of $^1O_2$ Generation

For $^1O_2$ detection, 2 mL of HB liposomes (25 μg/mL) were mixed with 100 μL DPBF solution. After US irradiation, the absorbance changes of DPBF at 410 nm were recorded.

4.2. ESR Measurement of $^1O_2$

For ESR measurement of ROS, $^1O_2$ generation was detected by TEMPO. Briefly, 1 mL of HB liposomes (50 μg/mL) was mixed with 20 μL TEMPO and exposed to US irradiation (1 W cm^2, 1.5 MHz) for 10 min. The characteristic peak signals were detected by an ESR spectrometer (Bruker, A300-12/10).

4.3. In Vitro Cellular Uptake

Colon 26 cells were seeded into a 96-well plate containing coverslips (1×10^5 cells per well) and incubated overnight for adherence. Next, 1 mL of RPMI 1640 containing Cy5-labeled HB liposomes was added to each well and incubated for 24 h. The fluorescence images were recorded using a CLSM.

4.4. Live/Dead Cell Staining Assay

Live/dead cell staining against Colon 26 cells was performed with the calcein-AM/PI solution. Colon 26 cells were grown in 6-well plates at a density of 1×10^5 cells per well, respectively. After 24 h incubation, cells were treated with vehicle or HB liposomes for 6 h. Then, the plates were exposed to US irradiation (3.0 MHz; 1.5 W cm^{-2}; 50% duty cycle) for 1 min. The plates were then incubated for another 12 h, after which the cells were washed three times with PBS and stained with 0.3 mL assay buffer containing calcein-AM (2.0 μM) and PI (4.5 μM). Subsequently, the cells were incubated for 30 min at 37 °C and

https://doi.org/10.1021/jacsau.3c00156
JACS Au 2023, 3, 1507−1520

observed using a CLSM. Live cells were stained green by calcein-AM, whereas the dead cells were stained red by PI.

4.5. Statistical Analysis

All data were presented as mean ± standard deviation (SD). Two-sided Student's *t*-test was carried out to assess two-group differences. In all the cases, statistical significance was set as follows: $*P < 0.05$, $**P < 0.01$, $***P < 0.001$, and not significant (N.S.).

■ ASSOCIATED CONTENT

Supporting Information

The Supporting Information is available free of charge at https://pubs.acs.org/doi/10.1021/jacsau.3c00156.

Additional experimental details for the material preparations, characterization data of materials, blood parameter data, and H&E staining (PDF)

■ AUTHOR INFORMATION

Corresponding Authors

Xin Sun − *Department of Cardiology, Shenzhen Cardiovascular Minimally Invasive Medical Engineering Technology Research and Development Center, and Shenzhen Clinical Research Centre for Geriatrics, Shenzhen People's Hospital, The First Affiliated Hospital, Southern University of Science and Technology, Shenzhen 518020 Guangdong, P. R. China*; Email: sunxinflying@163.com

Weihua Li − *Medical Imaging Department, Shenzhen Second People's Hospital/the First Affiliated Hospital of Shenzhen University Health Science Center, Shenzhen 518035, P. R. China*; Email: 18804511716163.com

Zhijie Li − *Department of Cardiology, Shenzhen Cardiovascular Minimally Invasive Medical Engineering Technology Research and Development Center, and Shenzhen Clinical Research Centre for Geriatrics, Shenzhen People's Hospital, The First Affiliated Hospital, Southern University of Science and Technology, Shenzhen 518020 Guangdong, P. R. China*; orcid.org/0000-0002-5445-7976; Email: li.zhijie@szhospital.com

Jigang Wang − *Department of Cardiology, Shenzhen Cardiovascular Minimally Invasive Medical Engineering Technology Research and Development Center, and Shenzhen Clinical Research Centre for Geriatrics, Shenzhen People's Hospital, The First Affiliated Hospital, Southern University of Science and Technology, Shenzhen 518020 Guangdong, P. R. China; Artemisinin Research Center, and Institute of Chinese Materia Medica, China Academy of Chinese Medical Sciences, Beijing 100700, P. R. China*; orcid.org/0000-0002-0575-0105; Email: jgwang@icmm.ac.cn

Authors

Haitao Yuan − *Department of Cardiology, Shenzhen Cardiovascular Minimally Invasive Medical Engineering Technology Research and Development Center, and Shenzhen Clinical Research Centre for Geriatrics, Shenzhen People's Hospital, The First Affiliated Hospital, Southern University of Science and Technology, Shenzhen 518020 Guangdong, P. R. China*; orcid.org/0000-0001-6141-7254

Jingbo Ma − *Department of Cardiology, Shenzhen Cardiovascular Minimally Invasive Medical Engineering Technology Research and Development Center, and Shenzhen Clinical Research Centre for Geriatrics, Shenzhen People's Hospital, The First Affiliated Hospital, Southern University of Science and Technology, Shenzhen 518020 Guangdong, P. R. China*

Wei Huang − *School of Chemical Engineering and Technology, Sun Yat-sen University, Zhuhai 519082, P. R. China*

Ping Gong − *Department of Emergency, Shenzhen People's Hospital, The First Affiliated Hospital, Southern University of Science and Technology, Shenzhen 518020 Guangdong, P. R. China*

Fei Shi − *Department of Infectious Disease, Shenzhen People's Hospital, The First Affiliated Hospital, Southern University of Science and Technology, Shenzhen 518020 Guangdong, P. R. China*

Xiaolong Xu − *Department of Cardiology, Shenzhen Cardiovascular Minimally Invasive Medical Engineering Technology Research and Development Center, and Shenzhen Clinical Research Centre for Geriatrics, Shenzhen People's Hospital, The First Affiliated Hospital, Southern University of Science and Technology, Shenzhen 518020 Guangdong, P. R. China*

Chunjin Fu − *Artemisinin Research Center, and Institute of Chinese Materia Medica, China Academy of Chinese Medical Sciences, Beijing 100700, P. R. China*

Xiaoxian Wang − *Department of Hyperbaric Oxygen Medicine, People's Hospital, The First Affiliated Hospital, Southern University of Science and Technology, Shenzhen 518020 Guangdong, P. R. China*

Yin Kwan Wong − *Department of Physiology, Yong Loo Lin School of Medicine, National University of Singapore, Singapore 117600, Singapore*

Ying Long − *Department of Hyperbaric Oxygen Medicine, People's Hospital, The First Affiliated Hospital, Southern University of Science and Technology, Shenzhen 518020 Guangdong, P. R. China*

Complete contact information is available at: https://pubs.acs.org/10.1021/jacsau.3c00156

Author Contributions

H.Y., J.M., W.H., P.G., and F.S. contributed equally to this work and conducted most of the experiments and produced figures. Y.L., X.S., Z.L., W.L., and J.W. designed and supervised the whole study and revised the manuscript. J.M., W.H., P. G., and F.S. helped with the biomedical evaluations and animal experiments. Y.W. and W.H. helped with the biological TEM measurement and structure analysis. J.M., P. G., W.H., and F.S. performed most of the immunofluorescence imaging/analysis. W.H., X.X., and X.W. performed nanoflow cytometry and helped with the cell experiments. C.F. analyzed RNA-seq data. H.Y., X.W., and J.M. constructed animal models. H.Y. and W.H. wrote the manuscript. All authors read and approved the final manuscript. CRediT: **Haitao Yuan** conceptualization, data curation, formal analysis, writing-original draft, writing-review & editing; **Jingbo Ma** formal analysis, methodology; **Wei Huang** formal analysis, methodology; **Ping Gong** supervision; **Fei Shi** supervision; **Xiaolong Xu** formal analysis; **Chunjin Fu** formal analysis; **XiaoXian Wang** formal analysis; **Yin Kwan Wong** formal analysis; **Ying Long** supervision; **Xin Sun** supervision; **Weihua Li** supervision; **Zhijie Li** formal analysis, supervision; **Jigang Wang** resources, supervision.

Notes

The authors declare no competing financial interest.

■ ACKNOWLEDGMENTS

This work was supported by the Shenzhen Science and Technology Innovation Commission (JCYJ20200109120205924), GuangDong Basic and Applied Basic Research Foundation (2021A1515012164), International Science and Technology Cooperation for Shenzhen Technology Innovation Plan (GJHZ20200731095411034), and National Key Research and Development Program of China (2020YFA0908000 and 2022YFC2303600). Chinese Postdoctoral Science Foundation (2022M712190) and GuangDong Basic and Applied Basic Research Foundation (2022A1515110745) to Y.H.T. Shenzhen Science and Technology Innovation Committee (SZSTI) (RCYX20221008092950121), the Science and Technology Foundation of Shenzhen (JCYJ20210324115800001); the Science and Technology Foundation of Shenzhen (Shenzhen Clinical Medical Research Center for Geriatric Diseases); Shenzhen Fund for Guangdong Provincial High-level Clinical Key Specialties (no. SZGSP001); Shenzhen Governmental Sustainable Development Fund (KCXFZ20201221173612034); Shenzhen key Laboratory of Kidney Diseases (ZDSYS201504301616234).

■ REFERENCES

(1) Li, M. O.; Wolf, N.; Raulet, D. H.; Akkari, L.; Pittet, M. J.; Rodriguez, P. C.; Kaplan, R. N.; Munitz, A.; Zhang, Z.; Cheng, S.; Bhardwaj, N. Innate immune cells in the tumor microenvironment. *Cancer Cell* **2021**, *39*, 725−729.

(2) Phuengkham, H.; Ren, L.; Shin, I. W.; Lim, Y. T. Nanoengineered Immune Niches for Reprogramming the Immunosuppressive Tumor Microenvironment and Enhancing Cancer Immunotherapy. *Adv. Mater.* **2019**, *31*, 1803322.

(3) Phuengkham, H.; Song, C.; Um, S. H.; Lim, Y. T. Implantable Synthetic Immune Niche for Spatiotemporal Modulation of Tumor-Derived Immunosuppression and Systemic Antitumor Immunity: Postoperative Immunotherapy. *Adv. Mater.* **2018**, *30*, 1706719.

(4) Gao, T.; Zhang, Z.; Liang, S.; Fu, S.; Mu, W.; Guan, L.; Liu, Y.; Chu, Q.; Fang, Y.; Liu, Y.; Zhang, N. Reshaping Antitumor Immunity with Chemo-Photothermal Integrated Nanoplatform to Augment Checkpoint Blockade-Based Cancer Therapy. *Adv. Funct. Mater.* **2021**, *31*, 2100437.

(5) Zeng, W.; Yu, M.; Chen, T.; Liu, Y.; Yi, Y.; Huang, C.; Tang, J.; Li, H.; Ou, M.; Wang, T.; Wu, M.; Mei, L. Polypyrrole Nanoenzymes as Tumor Microenvironment Modulators to Reprogram Macrophage and Potentiate Immunotherapy. *Adv. Sci.* **2022**, *9*, 2201703.

(6) Zhang, C.; Xia, D.; Liu, J.; Huo, D.; Jiang, X.; Hu, Y. Bypassing the Immunosuppression of Myeloid-Derived Suppressor Cells by Reversing Tumor Hypoxia Using a Platelet-Inspired Platform. *Adv. Funct. Mater.* **2020**, *30*, 2000189.

(7) Wang, Z.; Gong, X.; Li, J.; Wang, H.; Xu, X.; Li, Y.; Sha, X.; Zhang, Z. Oxygen-Delivering Polyfluorocarbon Nanovehicles Improve Tumor Oxygenation and Potentiate Photodynamic-Mediated Antitumor Immunity. *ACS Nano* **2021**, *15*, 5405−5419.

(8) Frank, D. A.; Mahajan, S.; Ritz, J. Fludarabine-induced immunosuppression is associated with inhibition of STAT1 signaling. *Nat. Med.* **1999**, *5*, 444−447.

(9) Meric-Bernstam, F.; Larkin, J.; Tabernero, J.; Bonini, C. Enhancing anti-tumour efficacy with immunotherapy combinations. *Lancet* **2021**, *397*, 1010−1022.

(10) Frohne, C. C.; Llano, E. M.; Perkovic, A.; Cohen, R. D.; Luke, J. J. Complete response of metastatic melanoma in a patient with Crohn's disease simultaneously receiving anti-α4α7 and anti-PD1 antibodies. *J. Immunother. Cancer* **2019**, *7*, 1.

(11) Hong, W.; Yang, J.; Bi, Z.; He, C.; Lei, H.; Yu, W.; Yang, Y.; Fan, C.; Lu, S.; Peng, X.; Wei, X. A mouse model for SARS-CoV-2-induced acute respiratory distress syndrome. *Signal Transduction Targeted Ther.* **2021**, *6*, 1.

(12) Zhou, F.; Feng, B.; Yu, H.; Wang, D.; Wang, T.; Ma, Y.; Wang, S.; Li, Y. Tumor Microenvironment-Activatable Prodrug Vesicles for Nanoenabled Cancer Chemoimmunotherapy Combining Immunogenic Cell Death Induction and CD47 Blockade. *Adv. Mater.* **2019**, *31*, 1805888.

(13) Du, Y.; Zhang, R.; Yang, J.; Liu, S.; Zhou, J.; Zhao, R.; He, F.; Zhang, Y.; Yang, P.; Lin, J. A "Closed-Loop" Therapeutic Strategy Based on Mutually Reinforced Ferroptosis and Immunotherapy. *Adv. Funct. Mater.* **2022**, *32*, 2111784.

(14) Gao, Z.; Jia, S.; Ou, H.; Hong, Y.; Shan, K.; Kong, X.; Wang, Z.; Feng, G.; Ding, D. An Activatable Near-Infrared Afterglow Theranostic Prodrug with Self-Sustainable Magnification Effect of Immunogenic Cell Death. *Angew. Chem., Int. Ed.* **2022**, *61*, No. e202209793.

(15) Jiang, W.; Wang, L.; Wang, Q.; Zhou, H.; Ma, Y.; Dong, W.; Xu, H.; Wang, Y. Reversing Immunosuppression in Hypoxic and Immune-Cold Tumors with Ultrathin Oxygen Self-Supplementing Polymer Nanosheets under Near Infrared Light Irradiation. *Adv. Funct. Mater.* **2021**, *31*, 2100354.

(16) Tan, X.; Huang, J.; Wang, Y.; He, S.; Jia, L.; Zhu, Y.; Pu, K.; Zhang, Y.; Yang, X. Transformable Nanosensitizer with Tumor Microenvironment-Activated Sonodynamic Process and Calcium Release for Enhanced Cancer Immunotherapy. *Angew. Chem., Int. Ed.* **2021**, *60*, 14051−14059.

(17) Tang, D.; Kepp, O.; Kroemer, G. Ferroptosis becomes immunogenic: implications for anticancer treatments. *OncoImmunology* **2021**, *10*, 1862949.

(18) Zheng, Y.; Li, X.; Dong, C.; Ding, L.; Huang, H.; Zhang, T.; Chen, Y.; Wu, R. Ultrasound-Augmented Nanocatalytic Ferroptosis Reverses Chemotherapeutic Resistance and Induces Synergistic Tumor Nanotherapy. *Adv. Funct. Mater.* **2022**, *32*, 2107529.

(19) Shen, F.; Tao, D.; Peng, R.; He, Y.; Liu, Z.; Ji, J.; Feng, L. Immunogenic nanomedicine based on GSH-responsive nanoscale covalent organic polymers for chemo-sonodynamic therapy. *Biomaterials* **2022**, *283*, 121428.

(20) Cao, F.; Sang, Y.; Liu, C.; Bai, F.; Zheng, L.; Ren, J.; Qu, X. Self-Adaptive Single-Atom Catalyst Boosting Selective Ferroptosis in Tumor Cells. *ACS Nano* **2022**, *16*, 855−868.

(21) Liu, T.; Liu, W.; Zhang, M.; Yu, W.; Gao, F.; Li, C.; Wang, S.-B.; Feng, J.; Zhang, X.-Z. Ferrous-Supply-Regeneration Nanoengineering for Cancer-Cell-Specific Ferroptosis in Combination with Imaging-Guided Photodynamic Therapy. *ACS Nano* **2018**, *12*, 12181−12192.

(22) Manigrasso, J.; Chillón, I.; Genna, V.; Vidossich, P.; Somarowthu, S.; Pyle, A. M.; De Vivo, M.; Marcia, M. Author Correction: Visualizing group II intron dynamics between the first and second steps of splicing. *Nat. Commun.* **2022**, *13*, 1.

(23) Ma, X.; Lee, C.; Zhang, T.; Cai, J.; Wang, H.; Jiang, F.; Wu, Z.; Xie, J.; Jiang, G.; Li, Z. Correction to: Image-guided selection of Gd@C-dots as sensitizers to improve radiotherapy of non-small cell lung cancer. *J. Nanobiotechnol.* **2022**, *20*, 1.

(24) Oh, J.-M.; Venters, C. C.; Di, C.; Pinto, A. M.; Wan, L.; Younis, I.; Cai, Z.; Arai, C.; So, B. R.; Duan, J.; Dreyfuss, G. U1 snRNP regulates cancer cell migration and invasion in vitro. *Nat. Commun.* **2020**, *11*, 1.

(25) Efimova, I.; Catanzaro, E.; Van der Meeren, L.; Turubanova, V. D.; Hammad, H.; Mishchenko, T. A.; Vedunova, M. V.; Fimognari, C.; Bachert, C.; Coppieters, F.; Lefever, S.; Skirtach, A. G.; Krysko, O.; Krysko, D. V. Vaccination with early ferroptotic cancer cells induces efficient antitumor immunity. *J. Immunother. Cancer* **2020**, *8*, No. e001369.

(26) Yin, Y.; Jiang, X.; Sun, L.; Li, H.; Su, C.; Zhang, Y.; Xu, G.; Li, X.; Zhao, C.; Chen, Y.; Xu, H.; Zhang, K. Continuous inertial cavitation evokes massive ROS for reinforcing sonodynamic therapy and immunogenic cell death against breast carcinoma. *Nano Today* **2021**, *36*, 101009.

https://doi.org/10.1021/jacsau.3c00156
JACS Au 2023, 3, 1507−1520

(27) Yue, W.; Chen, L.; Yu, L.; Zhou, B.; Yin, H.; Ren, W.; Liu, C.; Guo, L.; Zhang, Y.; Sun, L.; Zhang, K.; Xu, H.; Chen, Y. Checkpoint blockade and nanosonosensitizer-augmented noninvasive sonodynamic therapy combination reduces tumour growth and metastases in mice. *Nat. Commun.* **2019**, *10*, 2025.
(28) Dong, Y.; Dong, S.; Liu, B.; Yu, C.; Liu, J.; Yang, D.; Yang, P.; Lin, J. 2D Piezoelectric Bi_2MoO_6 Nanoribbons for GSH-Enhanced Sonodynamic Therapy. *Adv. Mater.* **2021**, *33*, 2106838.
(29) Liang, S.; Liu, B.; Xiao, X.; Yuan, M.; Yang, L.; Ma, P. a.; Cheng, Z.; Lin, J. A Robust Narrow Bandgap Vanadium Tetrasulfide Sonosensitizer Optimized by Charge Separation Engineering for Enhanced Sonodynamic Cancer Therapy. *Adv. Mater.* **2021**, *33*, 2101467.
(30) Deng, H.; Zhou, Z.; Yang, W.; Lin, L.-s.; Wang, S.; Niu, G.; Song, J.; Chen, X. Endoplasmic Reticulum Targeting to Amplify Immunogenic Cell Death for Cancer Immunotherapy. *Nano Lett.* **2020**, *20*, 1928−1933.
(31) Jiang, W.; Dong, W.; Li, M.; Guo, Z.; Wang, Q.; Liu, Y.; Bi, Y.; Zhou, H.; Wang, Y. Nitric Oxide Induces Immunogenic Cell Death and Potentiates Cancer Immunotherapy. *ACS Nano* **2022**, *16*, 3881−3894.
(32) Tao, N.; Li, H.; Deng, L.; Zhao, S.; Ouyang, J.; Wen, M.; Chen, W.; Zeng, K.; Wei, C.; Liu, Y.-N. A Cascade Nanozyme with Amplified Sonodynamic Therapeutic Effects through Comodulation of Hypoxia and Immunosuppression against Cancer. *ACS Nano* **2022**, *16*, 485−501.
(33) Yuan, M.; Liang, S.; Zhou, Y.; Xiao, X.; Liu, B.; Yang, C.; Ma, P. a.; Cheng, Z.; Lin, J. A Robust Oxygen-Carrying Hemoglobin-Based Natural Sonosensitizer for Sonodynamic Cancer Therapy. *Nano Lett.* **2021**, *21*, 6042−6050.
(34) Liang, S.; Xiao, X.; Bai, L.; Liu, B.; Yuan, M.; Ma, P. a.; Pang, M.; Cheng, Z.; Lin, J. Conferring Ti-Based MOFs with Defects for Enhanced Sonodynamic Cancer Therapy. *Adv. Mater.* **2021**, *33*, 2100333.
(35) Yuan, H.; Xia, P.; Sun, X.; Ma, J.; Xu, X.; Fu, C.; Zhou, H.; Guan, Y.; Li, Z.; Zhao, S.; Wang, H.; Dai, L.; Xu, C.; Dong, S.; Geng, Q.; Li, Z.; Wang, J. Photothermal Nanozymatic Nanoparticles Induce Ferroptosis and Apoptosis through Tumor Microenvironment Manipulation for Cancer Therapy. *Small* **2022**, *18*, 2202161.
(36) Yang, Y.; Ge, J.; Li, G.; Lei, H.; Chen, L.; Gong, Y.; Zhong, X.; Wang, L.; Dai, Y.; Tang, W.; Zou, J.; Cheng, Y.; Liu, Z.; Cheng, L. Manganese-doping titanium disulfide cascade nanobioreactors for sequential gas-sonodynamic strategy with immune checkpoint blockade therapy of cancer. *Nano Today* **2022**, *46*, 101585.
(37) Zhou, L.; Dong, C.; Ding, L.; Feng, W.; Yu, L.; Cui, X.; Chen, Y. Targeting ferroptosis synergistically sensitizes apoptotic sonodynamic anti-tumor nanotherapy. *Nano Today* **2021**, *39*, 101212.
(38) Liang, S.; Deng, X.; Ma, P. a.; Cheng, Z.; Lin, J. Recent Advances in Nanomaterial-Assisted Combinational Sonodynamic Cancer Therapy. *Adv. Mater.* **2020**, *32*, 2003214.
(39) Haze, K.; Yoshida, H.; Yanagi, H.; Yura, T.; Mori, K. Mammalian Transcription Factor ATF6 Is Synthesized as a Transmembrane Protein and Activated by Proteolysis in Response to Endoplasmic Reticulum Stress. *Mol. Biol. Cell* **1999**, *10*, 3787−3799.
(40) Liu, J.; Kuang, F.; Kroemer, G.; Klionsky, D. J.; Kang, R.; Tang, D. Autophagy-Dependent Ferroptosis: Machinery and Regulation. *Cell Chem. Biol.* **2020**, *27*, 420−435.
(41) Zhang, Y.; Tian, S.; Huang, L.; Li, Y.; Lu, Y.; Li, H.; Chen, G.; Meng, F.; Liu, G.; Yang, X.; Tu, J.; Sun, C.; Luo, L. Reactive oxygen species-responsive and Raman-traceable hydrogel combining photodynamic and immune therapy for postsurgical cancer treatment. *Nat. Commun.* **2022**, *13*, 4553.
(42) Pilard, C.; Ancion, M.; Delvenne, P.; Jerusalem, G.; Hubert, P.; Herfs, M. Cancer immunotherapy: it's time to better predict patients' response. *Br. J. Cancer* **2021**, *125*, 927−938.

https://doi.org/10.1021/jacsau.3c00156
JACS Au 2023, 3, 1507−1520